Heat Transfer and Fluid Flow Characteristics of Two-Phase Jet Impingement at Low Nozzle-to-Plate Spacing

by

Aspen W. Glaspell

Submitted in Partial Fulfillment of the Requirements

for the Degree of

Master of Science

in the

Mechanical Engineering

Program

YOUNGSTOWN STATE UNIVERSITY

August, 2018

Heat Transfer and Fluid Flow Characteristics of Two-Phase Jet Impingement at Low Nozzle-to-Plate Spacing

Aspen W. Glaspell

I hereby release this thesis to the public. I understand that thesis will be made available from the OhioLINK ETD Center and the Maag Library Circulation Desk for public access. I also authorize the University or other individuals to make copies of this thesis as needed for scholarly research.

Signature:

Aspen W. Glaspell, Student — Date

Approvals:

Dr. Kyosung Choo, Thesis Advisor — Date

Dr. Stefan I. Moldovan, Committee Member — Date

Dr. Kevin J. Disotell, Committee Member — Date

Dr. Salvatore A. Sanders, Dean of Graduate Studies — Date

ABSTRACT

This study expands upon the current knowledge of the relationship between the heat transfer and fluid flow characteristics of air-assisted water impingement jets. Fluid flow and heat transfer characteristics of air-assisted water jet impingement were experimentally investigated under a fixed water flow rate condition with varying relative height (H/d). The test fluids were water and air. The effects of nozzle-to-plate spacing at volumetric qualities β =0.3, 0.5, 0.7, and 0.8 where β is the ratio of the volume of air to the total volume of the two-phase mixture on the hydraulic jump diameter, stagnation pressure, and stagnation Nusselt number were considered. The results showed that stagnation Nusselt number, hydraulic jump diameter, and stagnation pressure increased as the relative height decreased and the volumetric quality increased with the maximum values occurring at H/d of 0.02 and a volumetric quality of 0.8. This research is most applicable in the use of cooling of industrial applications such as cooling of electronics and processing of materials.

CONTENTS

NOMENCLATURE

d	nozzle diameter [m]
D_h	hydraulic jump diameter [m]
g	gravitational acceleration [m/s^2]
H	nozzle to plate height [m]
K	jet deflection coefficient [-]
L	nozzle length [m]
P_0	pressure measured at stagnation point [kPa]
P^*_0	normalized pressure [-]
ΔP	pressure drop [Pa]
Pr	Prandtl number [ν/α]
Q	flow rate [m^3/s]
q	heat per unit volume [W]
r_{hj}	radius measured from jet stagnation point [m]
Re	Reynolds number [Ud/ν]
U	average velocity component along jet axis [m/s]
α	thermal diffusivity [m^2/s]
β	volumetric quality [-] the ratio of the flow rate of air to the total flow rate of the two-phase mixture
ρ	kinematic viscosity [kg/m^3]
ν	kinematic viscosity [m^2/s]

Subscripts

cond	conduction

conv	convection
a	air
f	fluid
gen	generated
hj	hydraulic jump
i	indexing value
loss	loss
rad	radiation
s	surface
stag	stagnation point
0	stagnation point
w	water
∞	ambient temperature

Superscripts

*	Dimensionless number

LIST OF FIGURES

CHAPTER I

INTRODUCTION AND BACKGROUND

Jet impingement is an attractive cooling mechanism due to the capability of achieving large heat transfer rates as shown in Figure 1. This cooling method has been used in diverse industrial applications such as annealing of metals, tempering of glass, cooling of gas turbine blades, cooling in grinding processes and cooling of photovoltaic cells. Examples of cooling metals, and cooling of gas turbine blades can be seen in Figures 2 and 3, respectively. Jet impingement has also become a viable candidate for high-powered electronic and photonic thermal management solutions and numerous jet impingement studies have been aimed directly at electronics cooling.

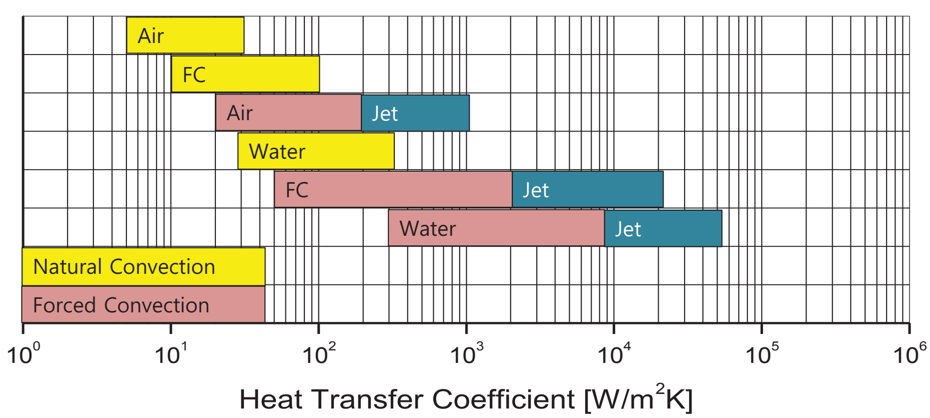

Figure 1: Heat transfer coefficient for impinging jets (Lasance and Simons, 2005).

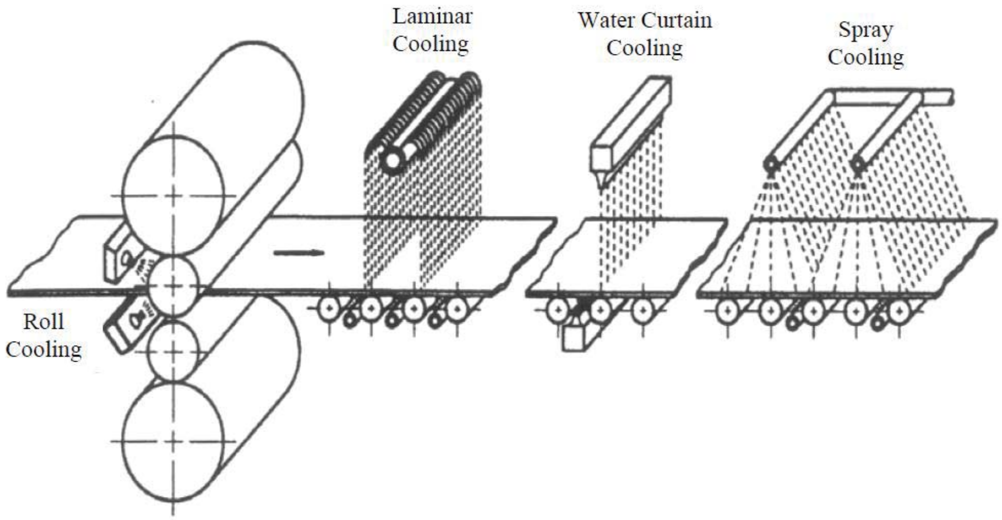

Figure 2: Applications of impinging jets for steel plate cooling (Zhao, 2005).

Figure 3: Airplane deicing (Wilson, 2018).

Active cooling by means of impinging jets offers an attractive alternative to conventional thermal management. Impinging jets offer the favorable characteristics of high local and area averaged heat transfer coefficients. As a result, impinging jets are ideal both for hot spot targeting or, if implemented in arrays, for global cooling. An illustration of jet arrays can be seen in Figure 4. Over the past 15 years, numerous studies Jaeger et al. (1989), Hollworth and Durbin (1992), Choi and Kim (1993), Korablev and Sharkov (1996), Marongiu and Maurice (1996), Stefanescu et al. (1999) have investigated jet impingement with direct application to thermal management. Air and water jets are well suited for cooling the heat exchangers that dissipates the heat to the ambient surroundings. As a result, it is prudent that impinging jet heat transfer and flow dynamics be investigated.

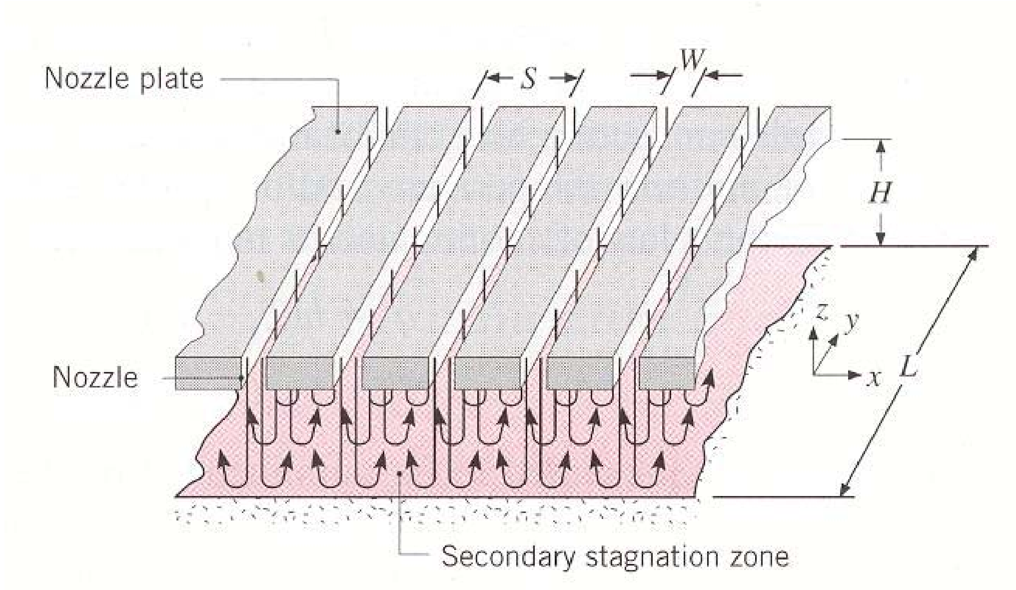

Figure 4: Surface impingement of an array of slot jets (Dickerson, 2016).

A significant body of literature exists for single circular impinging jet heat transfer and flow dynamics Goldstein et al. (1986), Garimella and Rice (1955), Garimella and Nenaydykh (1996). Generally, it has been determined that the magnitude and distribution of the heat transfer coefficient depends on several parameters including but not limited to the Reynolds number of the fluid (Re_f), Prandtl number of the fluid (Pr_f), nozzle-to-plate spacing (H/d), jet diameter (d), degree of confinement, as well as the physical geometry of the jets and target surface as stated by Goldstein and Timmers (1982), Baughn, and Shimizu (1989). The Reynolds number and Prandtl number are calculated in the equations below:

$$Re_f = \frac{Ud}{\nu} \tag{1}$$

$$Pr_f = \frac{\nu}{\alpha} \tag{2}$$

where U is the average velocity component along jet axis (m/s), d it the nozzle diameter (m), ν is kinematic viscosity (m^2/s), and α is the thermal diffusivity (m^2/s).

The hydraulic jump is a hydraulic phenomenon which is often observed in rivers and canals. The hydraulic jump is also observable in ordinary situations such as a typical household hose, as shown in Figure 5.

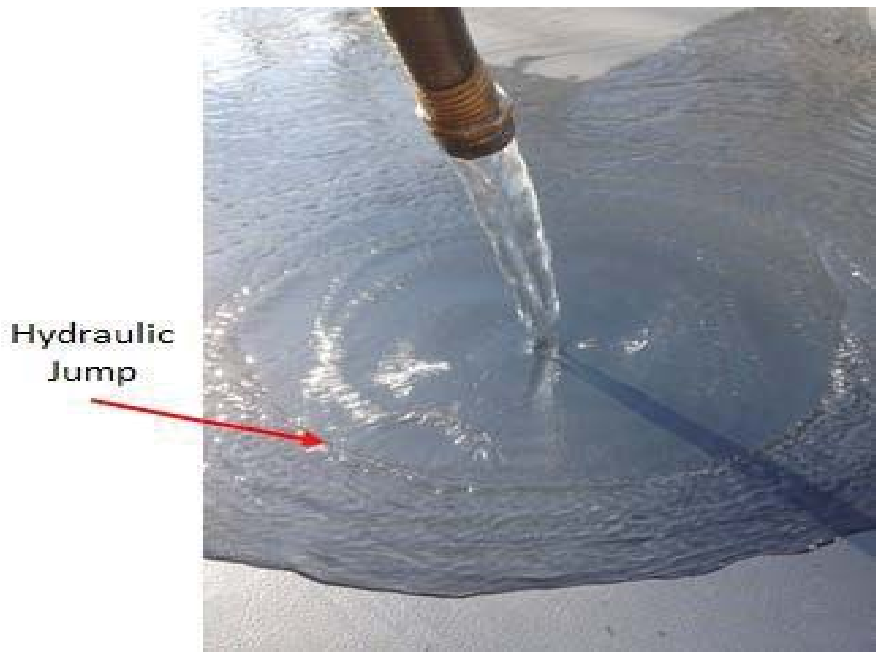

Figure 5: Hydraulic jump caused by a regular household hose.

High velocity liquid discharging into a zone of lower velocity causes an abrupt rise in the height of the liquid's surface. This phenomenon is mostly dependent on the initial fluid speed. When the critical speed is greater than the initial speed of the fluid, then a hydraulic jump will not form. When the critical speed is less than the initial speed a hydraulic jump forms. If a water jet impinges on a horizontal plate, at a certain distance away from the jet impact point a circular hydraulic jump is formed. The strength of the jump is dictated by boundary conditions both up and downstream. The strength of the jump will determine the type of hydraulic jump and its stability. When flow velocity is less than critical velocity, subcritical flow occurs. When flow velocity is greater than critical velocity, supercritical flow occurs. Figure 6 shows an example of a sluice gate which depicts a hydraulic jump, subcritical, and critical flow.

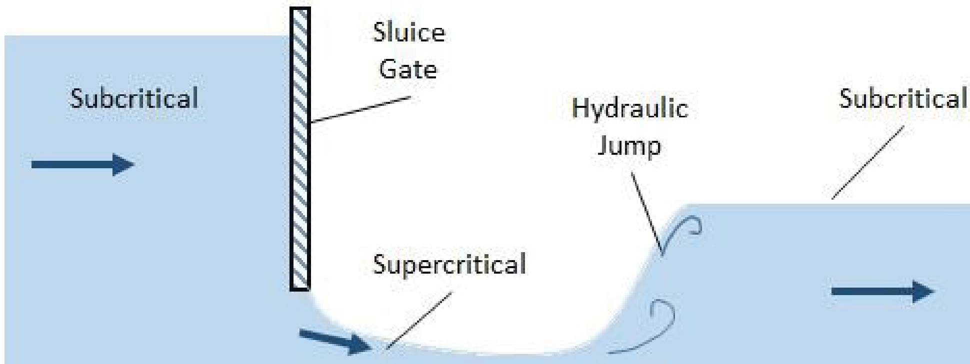

Figure 6: Hydraulic jump diagram (ME Case Studies, 2011).

The determination of the diameter of hydraulic jump is very important since the heat transfer characteristics of impinging jets are drastically changed at the location of hydraulic jump, as mentioned by previous researchers Baonga et al. (2006), Liu and Lienhard (1993), Stevens and Webb (1991). Due to the importance of hydraulic jump, extensive studies on the heat transfer and hydrodynamics of hydraulic jumps for single-phase impinging jets have been reported in the literature Chang et al. (2001), Chanson (2009), Craik et al. (1981), Godwin (1993), Louahlia-Gualous and Baonga (2008), Mikielewicz and Mikielewicz (2009), Watson (1964), Zhao and Khayat (2008).

The hydraulic jump is created using an impinging jet in this research. The impinging jet is a fluid flow that is directed by a nozzle and discharged at a surface where the fluid can be a liquid, gas or a mixture of both. In this research, the impinging jet was an unsubmerged jet, where the fluid passes through the ambient air before it impinges on the test surface. Upon contact with the surface it creates a turbulent region as shown in Figure 7, which becomes a hydraulic jump. Impinging jets are extremely efficient at transferring large amounts of thermal energy or mass between the fluid flow and the impinging surface. In high heat transfer applications where a large heat load needs to be removed, an impinging jet is an attractive solution due to its high heat flux. These high heat fluxes mostly depend on the velocity of the jet which will produce a high stagnation pressure Chang et al (2001). The high pressure creates a turbulent region after the impinging zone which offers a high heat transfer coefficient when compared to other conventional convection cooling methods. This heat transfer coefficient can be three times larger than other conventional convection cooling, such as parallel flow Lienhard (2001). Impinging jets are used in applications such as drying foods, cooling processed materials, cooling of electronics, cooling turbine engines, and cooling during machining and other industrial processes. A schematic diagram illustrating the different regions of an impinging jet are shown in Figure 7.

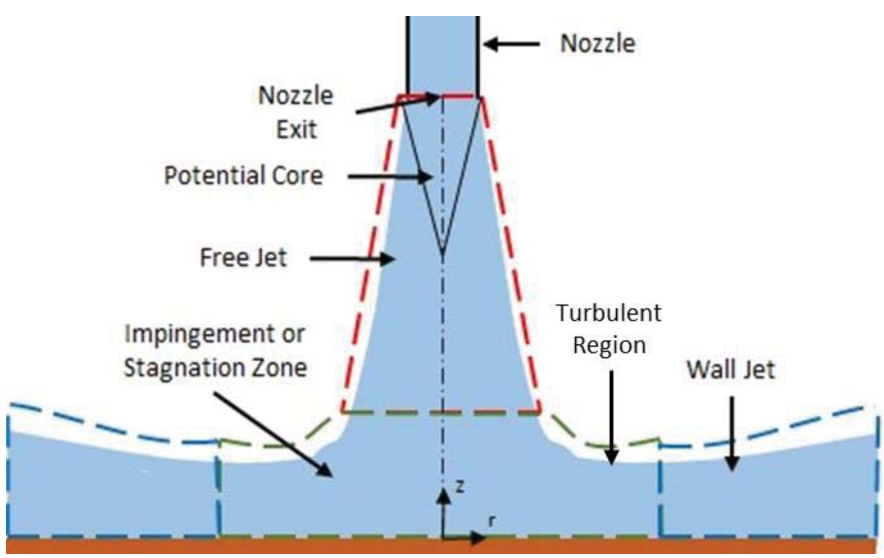

Figure 7: Impinging jet diagram (Incropera and DeWitt, 2009).

This experiment focuses on the fluid flow and heat transfer of the two-phase mixture of air and water. It is important that a proper understanding of the mechanics of fluids and heat transfer is required to understand the correlations of heat transfer and fluid flow. Heat transfer is the process by which heat that can be transferred from one system to another system of different temperature. The energy transfer is caused by the temperature difference between systems Cengel and Ghajar (2011). The focus of this research is convection. The phenomenon of interest in the heat transfer testing portion in this experiment is convection. Forced convection occurs when a fluid is forced over a surface by external means, as seen in Figure 8. This means that forced convection is closely tied with fluid mechanics Cengel and Chajar (2011).

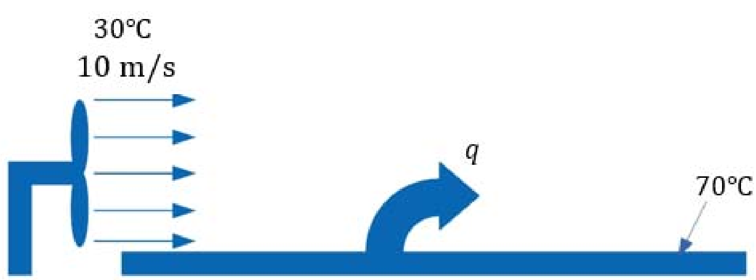

Figure 8: Forced Convection Example

Forced convection improves heat transfer. This occurs when either a warmer or cooler fluid is forced to make contact with a surface. This initiates higher rates of convection throughout the fluid compared to natural convection. Because of this, the greater the fluid velocity, the greater the heat transfer rate. Heat transfer via convection can be expressed as:

$$q = hA_s(T_s - T_\infty) \tag{3}$$

where h is the convection heat transfer coefficient ($W/m^2 \cdot K$), A_s is the heat transfer surface area (m^2), T_s is the surface temperature (ºC), and T_∞ is the fluid temperature (ºC). The convection heat transfer coefficient is defined as the rate of heat transfer between a solid surface and a fluid per unit surface area per unit temperature difference. In the case of convection, it is important to look at the ratio of convective to conductive heat transfer across the boundary (surface). That ratio creates the Nusselt number, Nu which is a dimensionless coefficient. The following equation defines the Nusselt number as:

$$Nu = \frac{hL_c}{k} \tag{4}$$

where L_c is the characteristic length (m) and k is the thermal conductivity of the fluid (W/m*K). The Nusselt number represents the degree of increase in heat transfer through a fluid layer as a result of convection relative to conduction across the same fluid layer, i.e., higher *Nu* leads to more effective convection, Cengel and Ghajar (2011).

A range of studies on applications of impinging jets have been performed. Webb and Ma (1995), Viskanta, (1993), Martin (1977), Polat et al. (1989) all researched single phase impinging jet flow for heat transfer characteristics. Lytle and Webb (1994) studied impinging jet flow at low nozzle-plate spacing H/d of 0.1 to 6. They found that decreasing nozzle height increases the heat transfer rate. Akansu et al. (2003), Abdel-Fattah and El-Baky (2009), Beitelmal et al. (2000), Yan and Saniei (1997) studied both numerical and experimental results for inclined impinging surfaces. They determined that when the angle is increased the largest heat transfer rate was found further higher along the inclined surface from the impinging zone. Several researchers have observed that the addition of a gas (or vapor) phase in an impinging liquid jet, which is considered a two-phase flow results in heat transfer enhancement. Zumbrunnen and Balasubramanian (1995) observed the enhancement in convection heat transfer caused by air bubbles injected into a planar water jet. Heat transfer was increased by almost 220% at the stagnation point over the range of liquid-only Reynolds number of $3{,}700 \leq Re_w \leq 21{,}000$ and the volumetric quality between $0 \leq \beta \leq 0.86$ where β is the ratio of the volume of air to the total volume of the two-phase mixture. Choo and Kim (2010) studied the heat transfer effects of an air-assisted impinging jet and obtained an optimum point, $\beta=0.2$, under a fixed pumping power condition. These researchers also noted that this enhancement had some costs associated with maintaining this enhancement. It was only feasible at operating conditions of a high pump power, due to system pressure drop and required flow rate. In addition, as the volumetric quality of the testing fluid at a constant flow rate was increased, the required power for pumping the water also increased as a direct result of increased pressure drop.

Although there have been previous studies on two phase impinging jets, the effect of volumetric quality with varying height on the relationship of Nusselt number, hydraulic jump, and stagnation pressure for two-phase impinging jets have not been thoroughly investigated.

The goal of this research is to determine the effects of the relative height ratio at several volumetric qualities of water with a constant flow rate on hydraulic jump diameter, stagnation pressure and stagnation Nusselt number for two phase impinging jets. The hydraulic jump diameter, stagnation pressure and Nusselt number were analyzed to determine their optimal values in relation to the relative height ratio. Air and water are the working fluids. A constant Re_w of 3262 was maintained for each of the relative height ratios from H/d = 0.02, 0.03, 0.05, 0.07, 0.09, 0.13, 0.17, 0.21, 0.26, 0.34, 0.43, and 0.51 at volumetric qualities of β = 0.3, 0.5, 0.7, and 0.8. Turbulent flow was chosen because it produces higher heat transfer rates compared to laminar flow. The findings from this study are most applicable to cooling applications such as thermal management for electronics. The experimental approach and data analysis are documented in Chapter 2. Chapter 3 describes the results and discussion. The conclusions and future directions for research are presented in Chapter 4.

CHAPTER II

EXPERIMENTAL APPROACH

The hydraulic jump diameter, and pressure caused by two-phase flow from an impinging jet were measured for a dimensionless nozzle-to-plate range of H/d of 0.02 to 0.51 with the water having a constant Reynolds number of 3262. The Reynolds number was kept constant by keeping the flow rate of the water at 14 GPH (gallons per hour). These measured values were used to calculate the stagnation Nusselt number of the two-phase flow.

2.1 FLOW SYSTEM

The flow path for both air and water are shown in schematic form in Figure 9.

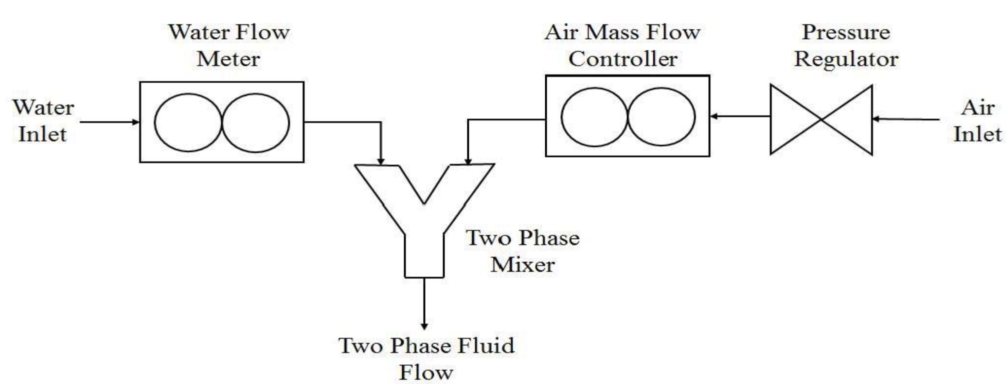

Figure 9: Schematic of test loop for air and water.

Before entering the two-phase mixer water and compressed air are channeled into flexible tubing. A photo of the two-phase mixer can be seen below in Figure 10. A schematic of the fluid flow set-up can be seen in Figure 11.

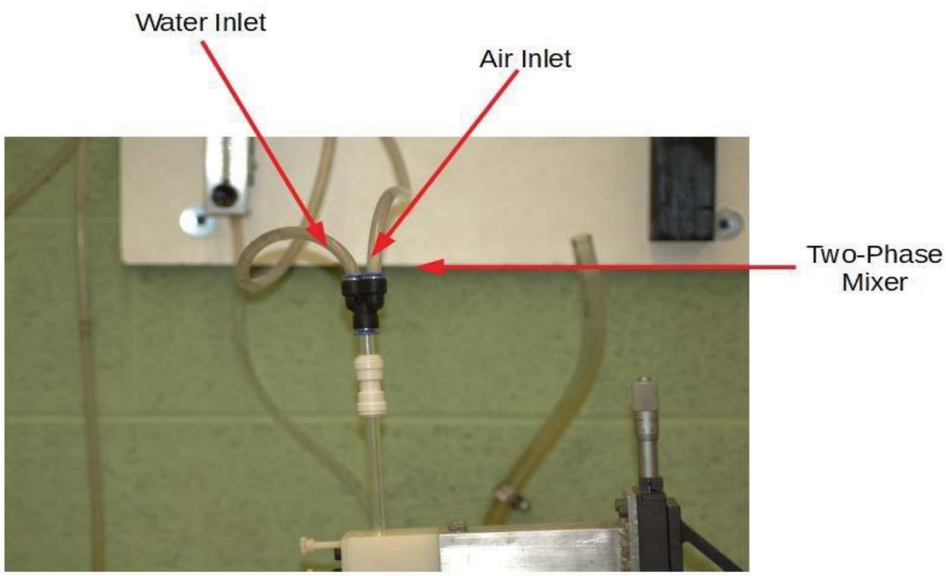

Figure 10: Two-phase mixer used in experiment.

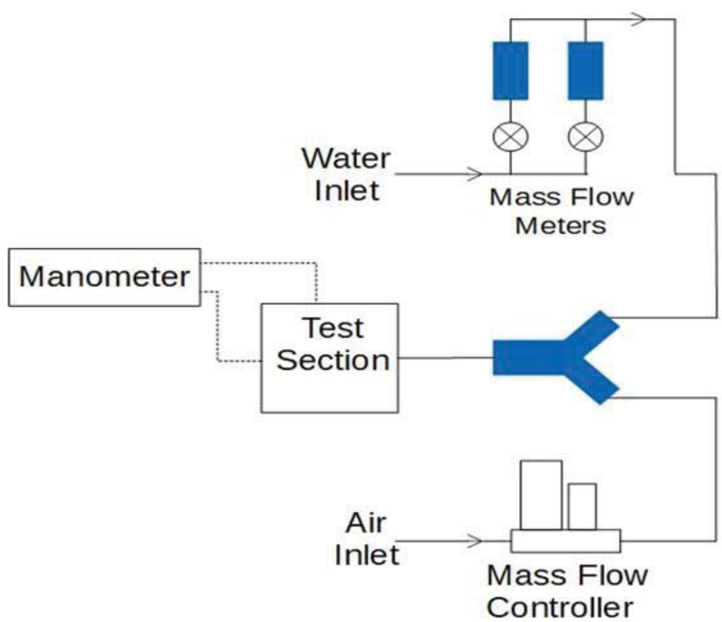

Figure 11: Schematic diagram of fluid flow experimental set-up.

A high-pressure tank is used to supply clean air at a steady flow rate using a pressure regulator. A mass flow controller (Omega FMA5520A), which had an accuracy of ±1% and a repeatability of ±0.15% was used to regulate and control the flow of air. The mass flow controller that was used had a range of 10 standard liters per minute. The working liquid was water which was pumped from a barrel reservoir. The liquid flow was regulated and controlled using a flowmeter valve (Dwyer RMB-84-SSV), and water pump (Micropump EagleDrive).

2.2 TEST ENVELOPE

For the fluid flow portion of the experiment, a circular, plastic nozzle which produced the impinging jet was used in the experiment after the two-phase mixer. The nozzle was 470 mm long with a diameter of 5.86 mm. Using a 3-axis (x-y-z) stage with a 10 μm resolution (Thorlabs, Inc, PT3A/M), the circular nozzle was kept in the same x-y position. The nozzle exit was positioned directly above the impinging surface. The nozzle-to-plate distance was adjusted by changing the height of the nozzle exit by adjusting only the z axis of the 3-axis stage. To measure the range of pressures from the impinging jet's stagnation zone a digital manometer (Meriam M2 Series) was used. As shown in Figure 19, the manometer had a range of 0 to 30 kPA with an accuracy of ±0.05%. The impinging jet's stagnation pressure was measured between the stagnation zone and the atmospheric pressure. The test apparatus was constructed from acrylic sheets. The impingement surface was designed at a higher elevation than the bottom pool so that the impinged liquid would fall off the impinging plate into the pool. This prevents disruptions from the downstream flow on the impinging fluid. The impinging plate was circular in shape and was made of a transparent acrylic sheet. The dimensions of the impinging plate are 5.15 mm thickness, 216 mm diameter, and 1 mm diameter orifice. Connected to the orifice was the manometer by the use of flexible tubing. A standard digital Vernier caliper was used to measure the hydraulic jump diameter. The diagram and photo of the fluid flow test section can be seen in Figures 12 (a) and 12 (b), respectively.

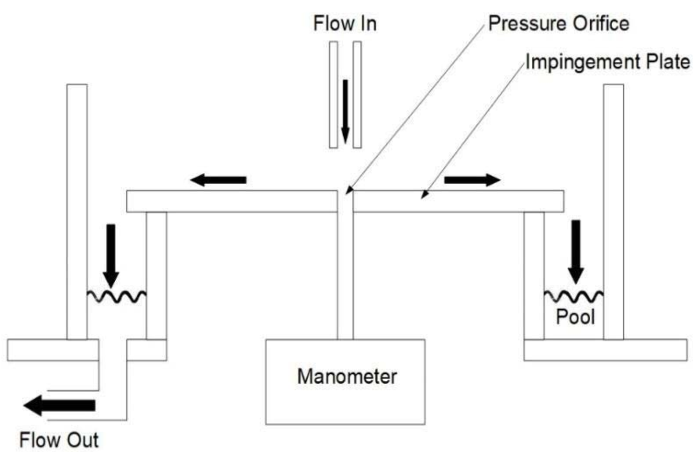

(a)

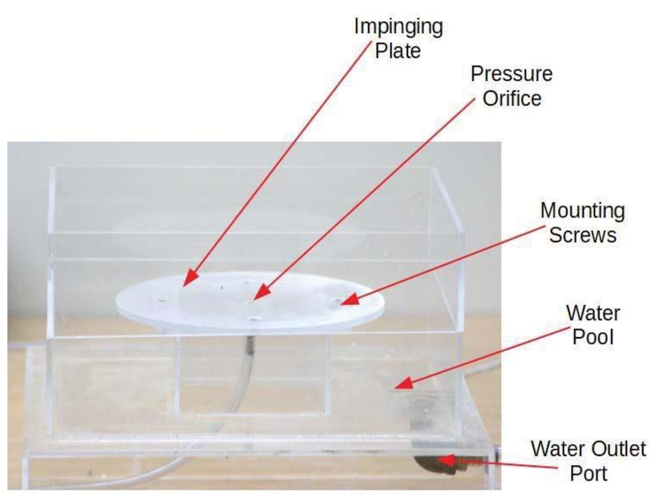

(b)

Figure 12: Fluids test section configuration: (a) cross sectional diagram of the test section and (b) actual test section used in the experiment.

To maintain uniformity of the test set-up during the heat transfer portion of the experiment, the fluid flow system going to the test section was left unchanged with only the fluid flow test section being replaced for the heat transfer test section. The heater was made of aluminum (0.0508 mm thick, 25 mm wide and 100 mm long). A DC power supply (Agilent 6651A #J03) was connected to the heater in series with a shunt rated 0-6 V and 0-60 A. Copper bus bars allowed adjustable DC voltage from the DC power supply to reach the heater. This was done by setting the current output to 50.707 A from the DC power supply. Fixing the current allowed the voltage output from the DC power supply to vary. When the temperature data was collected, the voltage output of the DC power supply was measured. Since DC electric current was applied to the heater, a nearly uniform wall heat flux boundary condition was created. Under steady state condition the amount of heat generation was calculated. The heat generation was the voltage across the heater multiplied by the current going into the heater. The diagram and photo of the heat transfer test section can be seen in Figures 14 (a) and 14 (b), respectively.

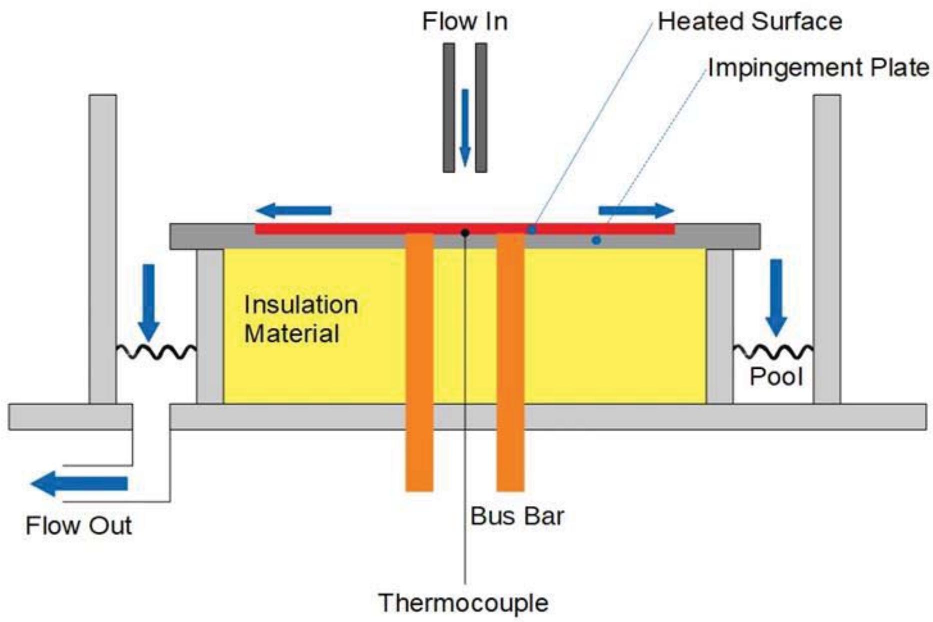

(a)

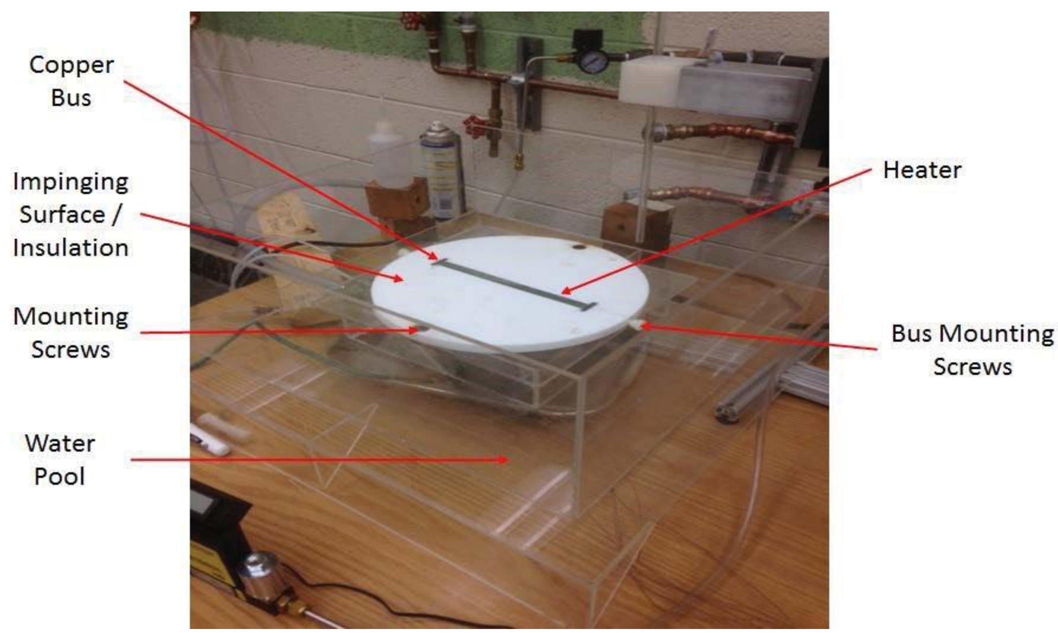

(b)

Figure 13: Heat transfer test set-up configuration: (a) cross sectional diagram of the test section and (b) actual test section used in the experiment.

The heater, thermocouple, and copper buses were mounted on a 12.7 mm thick PTFE Teflon disk. Also, the Teflon disc provided insulation to minimize heat loss through the bottom of the heater. One K-type thermocouple (with a max service temperature of 260°C) with a diameter 0.08 mm was fixed through a 1 mm mounting hole on the center of the Teflon disk by a high temperature thermal epoxy (with a max service temperature of 260°C). The Teflon disk's center was the same as the center of the rectangular test section. Directly laid over the thermocouple was a thin double sided adhesive strip with a hole for the thermocouple to go through. Then the heater was directly placed on top of the double sided adhesive strip so that it was in constant contact with the thermocouple. Connected to the thermocouple was an OMEGA OM-CP-QuadTemp2000 digital data acquisition system (DAQ). By connecting the DAQ to a computer, real-time temperatures were recorded at a sample rate of 1 reading per second. The bottom of the Teflon disk was not perfectly level because of the machining process. To address this, a heat resistant latex caulking (Nelson Latex Firestop Sealant) was used to seal the bottom of the Teflon disk to the test apparatus. Figure 14 shows a schematic of the heat transfer set-up.

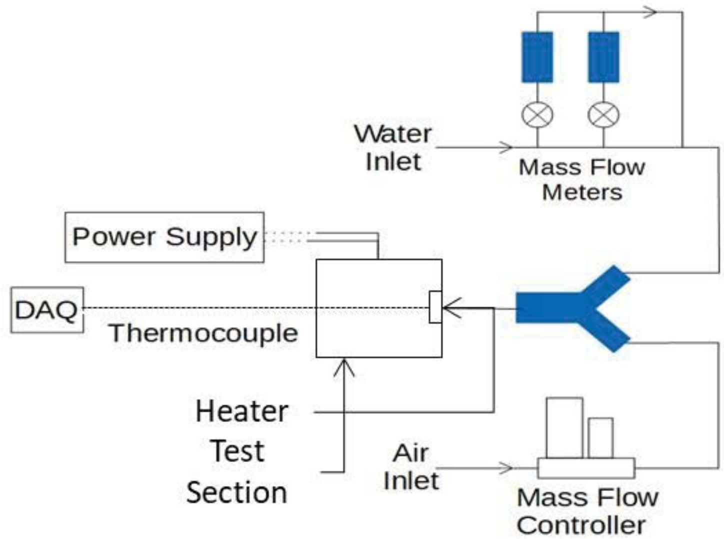

Figure 14: Diagram of heat transfer experimental set-up.

The fluid properties, resistance and surface area of the heater surface, power from the DC power supply, and the temperature data from the DAQ were used to calculate the Nusselt number at each relative height ratio, using equations (1) and (2).

2.3 PROCEDURE

For the fluid flow portion of the experiment, the hydraulic jump diameter and stagnation pressure were measured at 1-minute intervals between each relative height change for different volumetric qualities were performed to ensure that there was steady-state fluid flow. Standard digital Vernier calipers with an accuracy of ±0.001 mm were used to measure the hydraulic jump diameter. The hydraulic jump was measured at an angle of 90º along the horizontal centerline rectangular test section. The center of the rectangular test section was also the center of the hydraulic jump diameter. This was done for at each relative height to minimize error in the measurements.

The heat transfer tests began by impinging single-phase water onto the heater surface. Then voltage and current were applied to the heater. The voltage and current entering the heater was determined by the DC power supply. Next the temperature reading from the thermocouple had to stabilize with variations of ±0.1 ºC for 3 min, then the temperature value could start being recorded. From then on, the air was added to the fluid and the measurements were taken at 3-minute intervals for each relative height change for different volumetric flow qualities.

2.4 DATA ANALYSIS OF FLOW PARAMETERS

The Reynolds number of the water was determined by calculating the average jet velocity from the measured water flow rate. The jet velocity and the Reynolds number can be calculated using the equations below:

$$U = \frac{4Q}{\pi d^2} \tag{5}$$

$$Re_w = \frac{Ud}{\nu} \tag{6}$$

where Q and ν are flow rate of the water and kinematic viscosity, respectively. The impingement power was determined by the measured total flow rate and the normalized stagnation pressure as seen below:

$$I.P = Q \cdot P_0^* \tag{7}$$

where Q is the total flow rate of the water and air going into the two-phase mixer which is measured from the mass flow controller and flowmeter and the normalized stagnation pressure is calculated as seen below:

$$P_0^* = \frac{P_0}{P_{0,H/d=0.51}} \tag{8}$$

where P_0 is the measured value of the stagnation pressure and $P_{0,H/d=0.51}$ is the value of the stagnation pressure at H/d=0.51.

2.5 DATA ANAYLSIS OF HEAT TRANSFER PARAMETERS

The local convective heat transfer coefficient and corresponding Nusselt number for the i^{th} control volume were calculated using the following equations:

$$h_i = \frac{q_{conv,i}}{A_i(T_i - T_\infty)} \tag{9}$$

$$Nu_i = \frac{h_i d}{k_f} \tag{10}$$

For a given control volume, the convective heat $q_{conv,i}$ from the upper control volume surface was calculated using the following equations:

$$q = q_{gen,i} + q_{cond,i} - q_{rad,i}$$

$$q = \left(\frac{FVI - q_{loss}}{A}\right) A_i + (2\pi tk)\left\{\left[\left(\frac{r_{i+1} + r_i}{2}\right)\frac{dT}{dr}\right]_{i+1/2} - \left[\left(\frac{r_{i-1} + r_i}{2}\right)\frac{dT}{dr}\right]_{i-1/2}\right\} - \varepsilon_i \sigma A_i\left(T_i^4 - T_\infty^4\right) \tag{11}$$

where the convective area of the i^{th} control volume is,

$$A_i = \pi\left\{\left(\frac{r_{i+1} + r_i}{2}\right)^2 - \left(\frac{r_{i-1} + r_i}{2}\right)^2\right\} \tag{12}$$

In the analysis, the radiation heat $q_{rad,i}$ was calculated from the Stefan-Boltzmann equation and the result is less than 0.5% of the total imposed heat which was the voltage across the heater multiplied by the current going into the heater. The lateral heat losses $q_{loss,i}$ were obtained by measuring the temperature on the bottom of the Teflon disk and applying the Nusselt number correlation as seen in equations (9) and (10). The maximum heat losses from the heated surface to the ambient temperature via the bottom of the Teflon disk are estimated to be about 1% of the total imposed heat. In Eq. (11), F accounts for non-uniformity factor of the heating film and $F \approx 1$ is usually adopted for small slender shape of the film. The radial conduction $q_{cond,i}$ was determined by placing 3 thermocouples radial spaced 1mm apart from each other. The radial conductive $q_{cond,i}$ was determined to be negligible. A higher lateral conduction distorts the measurement accuracy of the surface temperature. Choo and Kim (2010) indicated that the lateral conduction along a heated plate increased the convective heat for an impinging jet. The lateral conduction has the same order of magnitude as the amount of heat supply to a heated foil which was used as a heater. In present study, the lateral conduction in the present study is less than 2% of the total imposed heat.

To estimate the errors present in the experimental results, an uncertainty analysis is conducted. The measurement error consists of bias and precision errors. The uncertainty *u.n.* is given as follows:

$$u.n. = \sqrt{b^2 - p^2} \tag{13}$$

where b and p are bias uncertainty and precision uncertainty, respectively. The precision uncertainty is determined by,

$$p = t_{95\%,n} \frac{S}{\sqrt{N}} \tag{14}$$

$$n = N - 1 \tag{15}$$

$$S = \sqrt{\frac{1}{N}\sum_{i=1}^{N}(x_i - \bar{x})^2} \tag{16}$$

where $t_{95\%,n}$, S, n, N, $\bar{x}$, and x_i are the t-distribution for a confidence level of 95%, standard deviation, degree of freedom, data number, sample mean, and measured value of particular experiment, respectively.

The uncertainty in the local Nusselt numbers is estimated with a 95 percent confidence level using the methods suggested by Kline and McKlintock (1953). Their methods calculate the uncertainty using the tolerances of the equipment being used in the experiment. The calculated maximum error of the main variables revealed an uncertainty of 2.7% for Nusselt number, 1.9% for the surface temperature, 1.2% for the inlet temperature at the nozzle exit, 1.1% for the heat loss, 1.1% for the input voltage, and 0.6% for the input current.

CHAPTER III

RESULTS AND DISCUSSION

3.1 VALIDATION

The experimental data of the Nusselt number in the present study for a free water impinging jet was compared with the empirical correlation of Steven and Webb (1991), Royne and Dey (2004) as a validation process. For Reynolds numbers in the range 4,023 $\leq Re_w \leq$ 8,053, the stagnation Nusselt numbers were examined at a nozzle-to-plate spacing of H/d = 1, as shown in Figure 15 (a). The adopted empirical correlation of Steven and Webb is $Nu = 3.62Re_w^{0.362}Pr^{0.4}$. As shown in the figure 15 (a), good agreements between the present data and the previous empirical correlation were observed within ± 10%. Validation for the stagnation pressure comes from the comparison of the single-phase liquid impingement data from Bernoulli's equation as shown in Figure 15 (b). The Bernoulli equation at stagnation point is given as:

$$P_o = \frac{1}{2}\rho U^2 + \rho g H \tag{17}$$

where P_0 is stagnation pressure and H is nozzle-to-plate spacing. The present data agrees with the experimental results of Brian K. Friedrich II and the Bernoulli's equation within ±10%. In addition, the measured hydraulic jump radius is validated with an empirical correlation of Brechet and Neda from Korablev and Sharkov (1996). The adopted empirical correlation is $r_{hj} = 0.8Q^{0.703}\nu^{-0.295}$. As shown in Figure 15 (c), good agreements between the present data and the previous empirical correlation were observed within ± 15% where the black line is the trend line.

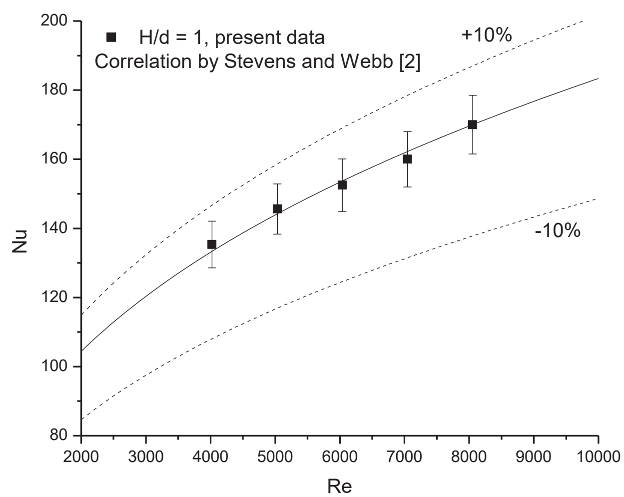

(a)

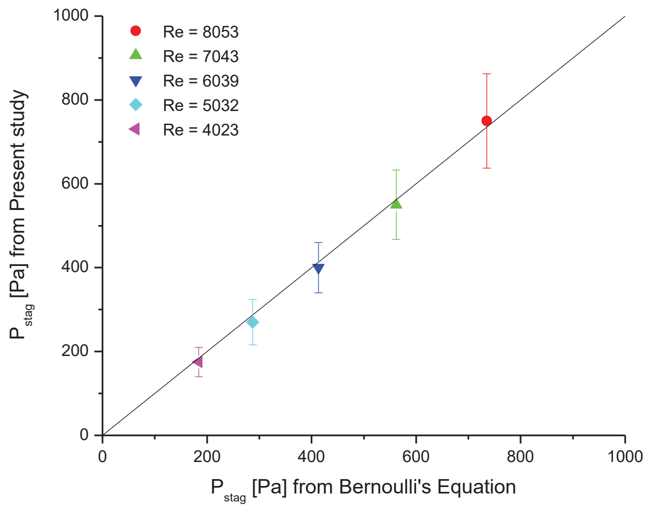

(b)

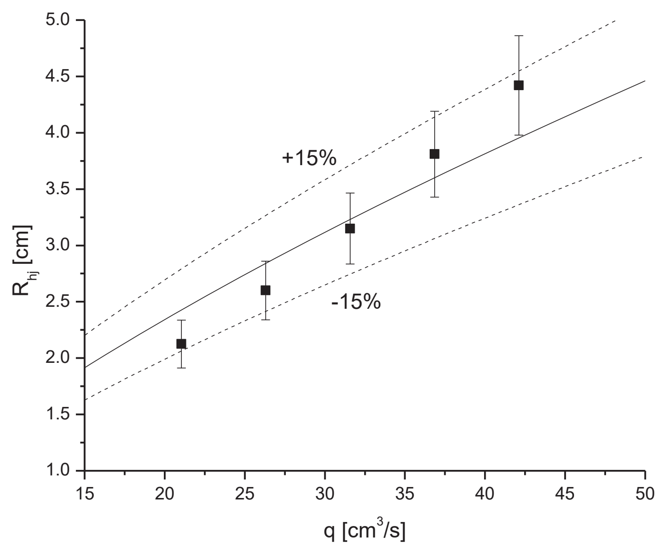

(c)

Figure 15: Validation for single phase water impinging jet: (a) stagnation Nusselt number (b) stagnation pressure (c) hydraulic jump diameter.

3.2 HYDRAULIC JUMP DIAMETER

The variation of the dimensionless hydraulic jump diameter with varying relative height ratio can be seen in Figure 16. The dimensionless hydraulic jump diameter is the measured hydraulic jump diameter divided by the nozzle diameter. The results are categorized into two regions; Region I is from H/d= 0.02 to 0.43, and Region II is from H/d =0.43 to 0.51.

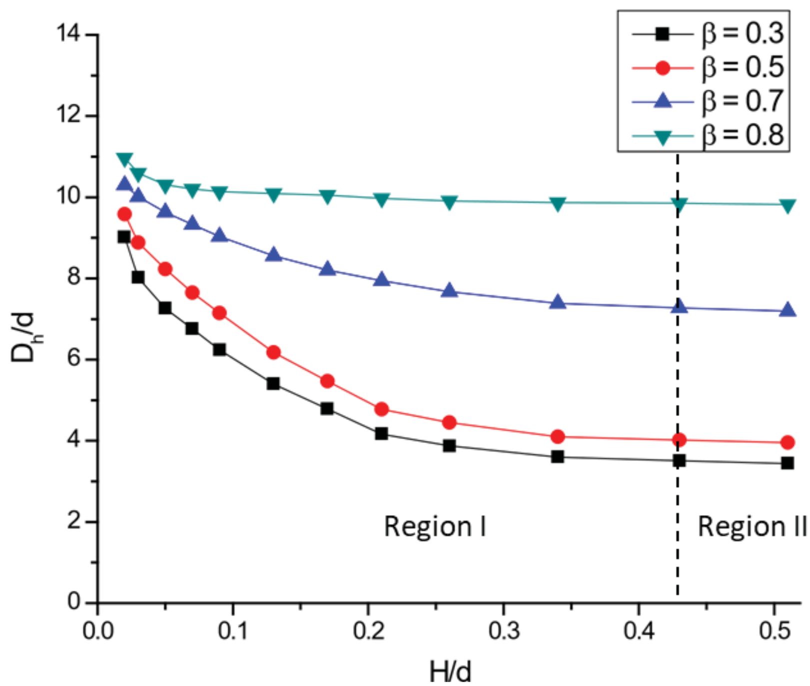

Figure 16: Hydraulic jump diameter as a function of the relative height ratio.

In Region I the dimensionless hydraulic jump diameter shows an exponential decrease as H/d increases towards Region II. This is because the normalized stagnation pressure decreases as H/d increases. In Region I the hydraulic jump diameter shows that as β increases the slope of the exponential curve decreases. The bubbles exiting the nozzle immediately diffuse into the ambient air at the lowest H/d value as seen in Figure 17 (a).

In Region II, there was a linear decrease in the hydraulic diameter until H/d reached 0.51. At that point the normalized stagnation pressure and the dimensionless hydraulic jump diameter approached their asymptotic values. The effect of β was the same on the dimensionless hydraulic jump diameter as it was in region I. In region II most of bubbles stayed intact and moved out of the hydraulic jump region as seen in Figure 17 (b). Figure 17 (b) shows a reduced hydraulic jump diameter compared to Figure 17 (a).

(a) H/d = 0.02 (b) H/d = 0.51

Figure 17: Nozzle discharge and hydraulic jump flow patterns for the minimum and maximum H/d at β= 0.5.

3.3 PRESSURE

Figure 18 shows the influence of the nozzle-to-plate spacing on the normalized stagnation pressure. The results show that the normalized stagnation pressure is divided into two regions: Region I, which is the jet deflection region ($H/d \leq 0.43$) and Region II, which is the inertia-dominant region ($0.43< H/d \leq 0.51$). The jet deflection region occurs when velocity is the dominant dominates the Bernoulli equation. The inertia-dominant region occurs when gravity is the dominates the Bernoulli equation.

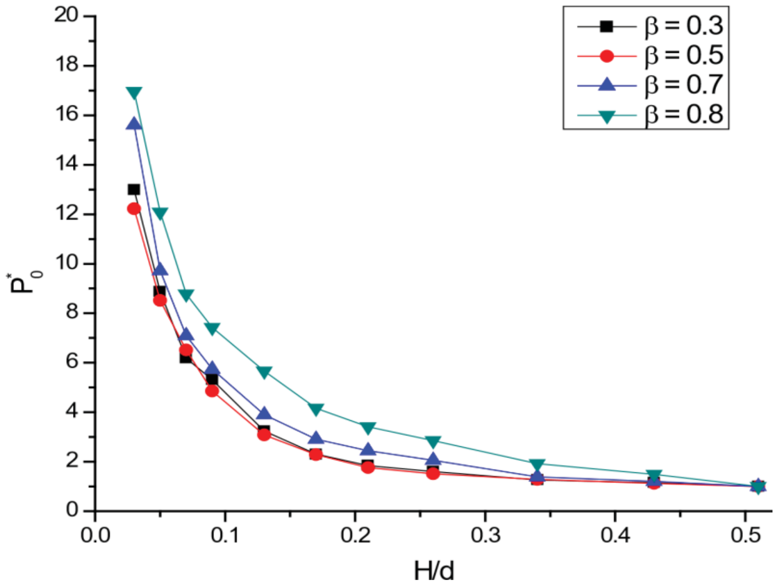

Figure 18: Normalized stagnation pressure as a function of the relative height ratio.

In region I, the normalized stagnation pressure drastically increases with decreasing the nozzle-to-plate spacing since flow resistance increases due to the flow deflection of the impinging plate. In region II, the effect of the nozzle-to-plate spacing is negligible on the normalized stagnation pressure. To explain the flow resistance of the flow deflection, an extended Bernoulli's equation is applied below:

$$P_0 = \frac{1}{2}\rho U_1^2 + \frac{K}{2}\rho U_2^2 \tag{18}$$

where K is jet deflection coefficient, which is empirically obtained from Figure 18 using trend lines. As the jet deflection coefficient increases the normalized stagnation increases and as the jet deflection coefficient decreases the normalized stagnation decreases. The pressure at stagnation point includes two effects, one from dynamic pressure at point 1 and another from the jet deflection effect at point 2 as shown in Figure 19. From the mass conservation equation, Eq. (19), at points 1 and 2, Equation (18) can be transformed as a function of nozzle-to-plate spacing only as shown in Eq. (20).

$$U_1\left(\frac{\pi d^2}{4}\right) = U_2(\pi d H) \tag{19}$$

$$P_0^* = \frac{P_0}{\frac{1}{2}\rho U_1^2} = 1 + \frac{K}{16}\left(\frac{H}{d}\right)^{-2} \tag{20}$$

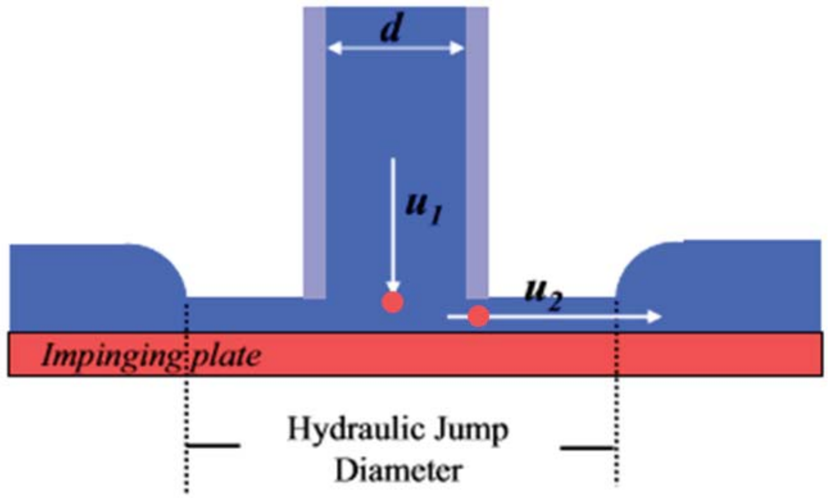

Figure 19: Notation for the velocity at low nozzle-to-plate spacing (Kuraan, Choo, and Moldovan).

3.4 NUSSELT NUMBER

The variation of stagnation Nusselt number with changing height to diameter ratio are shown in Figure 20. The results are similar to the hydraulic jump and can be broken up into two regions; Region I is from H/d = 0.02 to 0.43, Region II is from H/d =0.43 to 0.51.

In region I in the stagnation Nusselt number exponentially decreases as H/d increases towards Region II. This decrease is occurring because the impinging power of the two-phase flow is decreasing as H/d increases. In region I the magnitude of Nu_0 increases as β increases. This is due to the flow pattern in the nozzle changing as β increased. The flow pattern in the nozzle was bubbly flow at β = 0.3, slug flow at β = 0.5, and annular flow at β = 0.8. The peak Nu_0 occurred at an H/d of 0.02 and at β of 0.8.

In region II in the stagnation Nusselt number linearly decreases as H/d increases to 0.51. The stagnation Nusselt number approached its asymptotic value linearly as H/d increased. As in region I, the magnitude of Nu_0 increases as β increases.

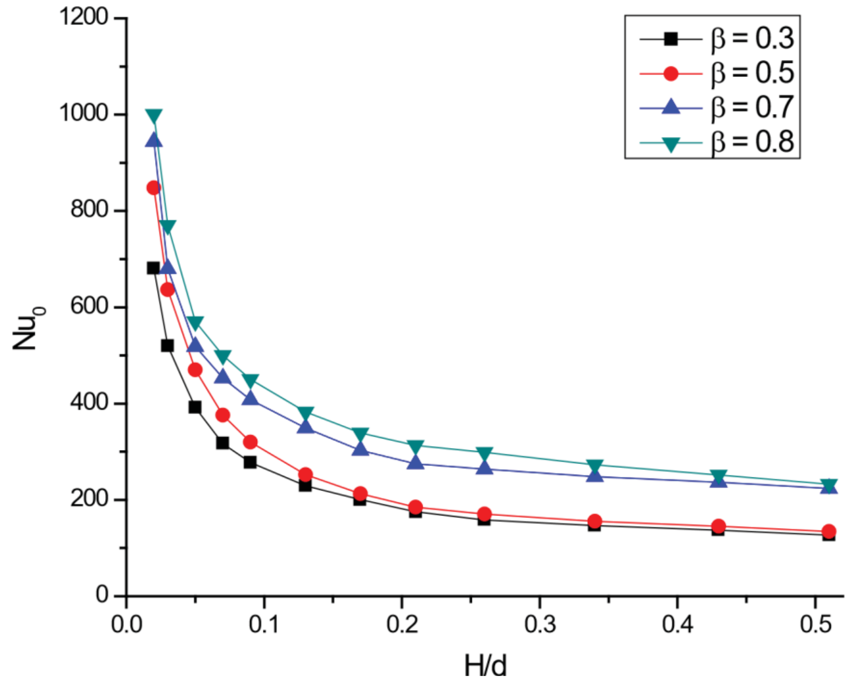

Figure 20: Stagnation Nusselt number as a function of the relative height ratio.

CHAPTER IV

CONCLUSIONS AND FUTURE WORK

Using water and air as the test fluid, the heat transfer characteristics of air-assisted water jet impingement were experimentally investigated in this study. The effects of varying nozzle-plate spacing at several different volumetric qualities (β = 0.3, 0.5, 0.7, and 0.8) on the Nusselt number and pressure were considered under fixed water-flow-rate condition. One fixed flow rate of 14 GPH was considered with Reynolds number for water of 3262 using the nozzle diameter as the characteristic length. A nozzle diameter of 5.86 mm was used to direct the impinging jet normal to the surface of the impinging surface at a range of height-to-diameter ratios from 0.02 to 0.51.

The results can be sorted into two regions; Region I is from H/d = 0.02 to H/d = 0.43, Region II is from H/d = 0.43 to 0.51. In region I, stagnation Nusselt number increased exponentially as H/d was decreased. The reason for the exponential increase in stagnation Nusselt number as H/d decreased was that by decreasing the nozzle-to-plate height, the velocity of the fluid in the stagnation zone increased to compensate for the reduced outlet area to adhere to the conservation of mass. The 90º bend in flow and the increased velocity in the extended Bernoulli equation increased the normalized stagnation pressure which increased the impingement power which increased the stagnation Nusselt number. In region II, the stagnation Nusselt number approached its asymptotic value linearly as H/d increased. This too is caused by the stagnation zone velocity changing in response to the increasing nozzle-to-plate spacing. This region also ends at the stable minimum location for the stagnation Nusselt number after which all values for the stagnation Nusselt number are the same.

The findings of this study are most useful for cooling applications such as electronics cooling to increase the overall heat transfer performance. Future studies could build upon this research by investigating the effect of surface conditions on two-phase impinging jet flow. Future work should address the limitations of this study. The limitations were caused by a lack of specific equipment needed to directly measure the velocity in the pipe and allow the heater to reach temperatures greater than 60ºC. The velocity of the two-phase mixture in the pipe could not be determined with the available lab equipment so the velocity was approximated with the known inlet velocities of the water and the air using conservation of mass. Future research could use the exact inlet velocity to precisely determine the effects of the bubble flow with the varying nozzle-to-plate spacing. The power supply used and the possible risk of damage to the heater and the plate itself limited the heater temperature. Increasing the heater temperature would allow for more extreme temperature differences which could increase the range of the results.

CHAPTER V

REFERENCES

Abdel-Fattah, A., M. Abd El-Baky, Numerical investigation of impinging two dimensional on an inclined flat plate, International Journal of Fluid Mechanics Research 35 (2009) 391-413.

Abdel-Fattah, A., Numerical and experimental study of turbulent impinging twin-jet flow, Experimental Thermal and Fluid Science 31 (2007) 1061-1072.

Akansu, Y.E., M. Sarioglu, K. Kuvvet, T. Yavuz, Flow field and heat transfer characteristics in an oblique slot jet impinging on a flat plate, Int. Communications in Heat Mass Transfer 35 (2008) 873-880.

Al-Hadhrami, L.M., S.M. Shaahid, Ali Mubarak, Heat transfer in a channel with inclined target surface cooled by single array of impinging jets, Proceedings of the ASME Turbo Expo, Montreal, Canada (2007) 35-42.

Al-Hadhrami, L.M., Study of heat transfer distribution in a channel with inclined target surface cooled by a single array of staggered impinging jets, Heat Transfer Engineering 31 (2010) 234-242.

Baonga, J.B., H. Louahlia-Gualous, M. Imbert, Experimental study of the hydrodynamic and heat transfer of free liquid jet impinging a flat circular heated disk, Appl. Therm. Eng. 26 (2006) 1125–1138.

Babic, D., D. B. Murray, A. A. Torrance, Mist Jet Cooling of Grinding Processes, Int. J. Mach. Tools Manufacturing 45 (2005) 1171-1177.

Baughn, J. W., S.S. Shimizu, Heat transfer measurements from a surface with uniform heat flux and an impinging jet, ASME Journal of Heat Transfer 111 (1989) 1096-1098.

Baydar, E., Y. Ozmen, An experimental investigation on flow structures of confined and unconfined impinging air jets, Heat Mass Transfer 42 (2006) 338-346.

Beitelmal, A.H., M.A. Saad, C.D. Patel, The effect of inclination on the heat transfer between a flat surface and an impinging two-dimensional air jet, International Journal of Heat and Fluid Flow 21 (2000) 156-163.

Bush, J.W.M., J.M. Aristoff, A.E. Hosoi, An Experimental investigation of the stability of the circular hydraulic jump, J. Fluid Mech. 558 (2006) 33-52.

Cengel, Yunus A., and Afshin J. Ghajar. Heat and Mass Transfer: Fundamental and Applications. New Delhi: McGraw Hill Education, 2011. Print.

Chang, C.T., G. Kojasoy, F. Landis, and S. Downing, Confined single- and multiple-jet impingement heat transfer—II. Turbulent two-phase flow, Int. J. Heat Mass Transfer 38 (1995) 843–851.

Chang, H. C., E.a. Demekhin, P.v. Takhistov, Circular Hydraulic Jumps Triggered by Boundary Layer Separation, Journal of Colloid and Interface Science 233.2 (2001): 329-338.

Chanson, H., Current knowledge in hydraulic jumps and related phenomena. A survey of experimental results, Eur. J. Mech. B/Fluids 28 (2009) 191–210.

Choi, S.B., W. T. Kim, Air jet impingement cooling of simulated multichip modules in the electronics, American Society of Mechanical Engineers, EEP, 4(2), (1993) 679-683.

Choo, K., Friedrich B. K., A.W. Glaspell, K. Schilling, “The Influence of Nozzle-to-plate Spacing on Heat Transfer and Fluid Flow of Submerged Jet Impingement,” International Journal of Heat and Mass Transfer 97 (2016), 66 – 69.

Choo, K., S. J. Kim, Heat transfer and fluid flow characteristics of two-phase impinging jets, International Journal of Heat and Mass Transfer 53 (2010) 5692-5699.

Choo, K., S.J. Kim, Heat Transfer and Fluid Flow Characteristics of Nonboiling TwoPhase Flow in Microchannels, ASME Journal of Heat Transfer 133 (2011) 102901.

Choo, K., S.J. Kim, The influence of nozzle diameter on the circular hydraulic jump of liquid jet impingement, Experimental Thermal and Fluid Science 72 (2016) 12–17.

Craik, A., R. Latham, M. Fawkes, P. Gibbon, The circular hydraulic jump, J. Fluid Mech. 112 (1981) 347–362.

Dickerson, B., Example of Multiple Jet Impingement Design: Slot Jet Array, https://slideplayer.com/slide/5820269/19/images/24/Example+of+Multiple+Jet+Impingent+Design:+Slot+Jet+Array.jpg (2016).

Friedrich, B. K., A. W. Glaspell, K. Choo, The Hydraulic Jump of Air-assistant Circular Impinging Jets, Experimental Thermal and Fluid Science, Under review.

Gardon, R., J.C. Akfirat, “Heat transfer characteristics of impinging two dimensional air jets,” J. Heat Transfer, 88, pp. 101-108, (1966).

Gardon, R., J.C. Akfirat, “The role of turbulence in determining the heat transfer characteristics of impinging jets,” Int. J. Heat Mass Transfer, 8, pp. 1261-1272, (1965).

Garimella, S., Air cooling technology for electronic equipment, CRC Press, 1996.

Garimella, S. V., and R. A. Rice, Confined and submerged liquid jet impingement heat transfer, ASME Journal of Heat Transfer, 117 (1955) 871-877.

Garimella, S. V., B. Nenaydykh, Nozzle geometry effects in liquid jet impingement heat transfer, International Journal of Heat and Mass Transfer 39 (1996) 2915-2923.

Godwin, R.P., The hydraulic jump (‘‘shocks” and viscous flow in the kitchen sink), Am. J. Phys. 61 (9) (1993) 829–832.

Goldstein, R. J., A. I. Behbahani, and K. Heppelmann, Streamwise distribution of the recovery factor and the local heat transfer coefficient to an impinging circular air jet, International Journal of Heat and Mass Transfer, 29, (1986) 1227-1235.

Goldstein, R.J., M.E. Franchett, Heat transfer from a flat surface to an oblique im-pinging jet, ASME J. Heat Transfer 110 (1988) 84-90.

Goldstein, R. J., J. F. Timmers, Visualization of heat transfer from arrays of impinging jets, International Journal of Heat and Mass Transfer 25 (1982) 1857-1868.

Hall, D.E., F.P. Incropera, R. Viskanta, Jet impingement boiling from a circular free surface jet during quenching; Part 2 – two-phase jet, ASME J. Heat Transfer 123 (2001) 911-917.

Hollworth, B. R., M. Durbin, Impingement Cooling of Electronics, Journal of Heat Transfer, ASME 114, (1992) 607-613.

Incropera, Frank P., and David P. DeWitt, Fundamentals of Heat and Mass Transfer, New York: J. Wiley & Sons, 2002. Print.

Jaeger, R.C., J. S. Goodling, M. E. Baginski, C. D. Ellis, N. V. Williamson, R. M. O'Barr, High heat flux cooling for silicon hybrid multichip packaging, IEEE transactions on components, hybrids, and manufacturing technology 12 (4) (1989) 772-779.

Johnson, M., D. Maynes, J. Crockett, Experimental characterization of hydraulic jump caused by jet impingement on micro-patterned surfaces exhibiting ribs and cavities, Experimental Thermal and Fluid Science 58 (2014) 216-223

Kline, S.J., F.A. McClintock, Describing uncertainties in single sample experiments, Mech. Eng. 75 (1) (1953) 3–8.

Korablev, V.A., A. V. Sharkov, 1996, Jet air and liquid cooling of electronic, Heat Transfer Research, 27(1) (1996) 1-3.

Kuraan A. M., K. Choo, S. I. Moldovan, Heat Transfer and hydrodynamics of free water jet impingement at low nozzle-to-plate spacings, International Journal of Heat and Mass Transfer 108 (2017) 2211-2216.

Lee, D.H., S.J. Kim, Y. H. Kim, H. J. Park, Heat transfer with fully developed slot jets impinging on confined concave and convex surfaces, Int. J. Heat and Fluid Flow 88 (2015) 218-223.

Lienhard, John H., (Mech Eng Mit) 2376 2001 Oct 19 12:23:28. C:textindia_2006jets.dvi (n.d.)

Liu, X., J.H. Lienhard, The hydraulic jump in circular jet impingement and in other thin liquid films, Exp. Fluids 15 (1993) 108–116.

Louahlia-Gualous, H., J.B. Baonga, Experimental study of unsteady local heat transfer for impinging miniature jet, Heat Transfer Eng. 29 (9) (2008) 782–792.

Lytle, D., B.W. Webb, Air jet impingement heat transfer at low nozzle-plate spacings, Int. J. Heat Mass Transfer 37 (1994) 1687-1697.

Marongiu, J. Maurice, Enhanced impingement cooling using nozzles with modified exit geometries for active heat sinks, Proceedings of the Intersociety Energy Conversion

Engineering Conference, 2 (1999) 1378-1383.

Martin, H., Heat and mass transfer between impinging gas jets and solid surface, Adv. Heat Transfer 13 (1977) 1-60.

Maynes, D., M. Johnson, B.W. Webb, Free-surface liquid jet impingement on rib patterned superhydrophobic surfaces, Physics of Fluids 23 (2011) 052104.

ME Case Studies, FM3 Hydraulic Jump through a Sluice Gate, N.p., 15 October 2011.

Web. 07 Apr. 2016.

Mikielewicz, J., D. Mikielewicz, A simple dissipation model of circular hydraulic jump, Int. J. Heat Mass Transfer 52 (2009) 17–21.

Mubarak, Ali, S.M. Shaahid, Luai M. Al-Hadhrami, Impact of jet Reynolds number and feed channel geometry on heat transfer in a channel with inclined target surface cooled by single array of centered impinging jets with outflow in both directions, Proc. of International Conference of Mechanical Engineering, London, U.K, (2011) 6-8.

Narumanchi, S. V. J., C. H. Amon, J. Y. Murthy, Influence of Pulsating Submerged Liquid Jets on Chip-Level Thermal Phenomena, Transactions of the ASME 125 (2003) 354-361.

Obot, N.T., W.J.M. Douglas, A.S. Majumdar, Effect of semi confinement on impingement heat transfer, Procs. 7th Int. Heat Transfer Conf. 3 (1982) 395-400.

Pence, D.V., P.A. Boeschoten, J.A. Liburdy, Simulation of compressible micro-scale jet impingement heat transfer, ASME J. Heat Transfer 125 (2003) 447-453.

Polat, S., B. Huang, A.S. Majumdar, W.J.M. Douglas, Numerical flow and heat transfer under impinging jets: A Review, Ann. Rev. Num. Fluid Mech. Heat Transfer 2 (1989) 157-197.

Royne, A., and C. Dey, Experimental Study of a Jet Impingement Device for Cooling of Photovoltaic Cells Under High Concentration, Proceedings of Solar 2004: Life, the Universe and Renewables.

Serizawa, A., O. Takahashi, Z. Kawara, T. Komeyama, I. Michiyoshi, Heat transfer augmentation by two-phase bubbly flow impinging jet with a confining wall, Proceedings of the 9th Int. Heat Transfer Conference, Jerusalem, 1990, pp. 93–98.

Stefanescu, S., M. Mehregany, J. Leland, K. Yerkes, Micro jet array heat sink for power electronics, Proceedings of the IEEE Micro Electro Mechanical Systems (MEMS) (1999) 165-170.

Stevens, J., B.W. Webb, Local heat transfer coefficients under an axisymmetric, singlephase liquid jet, ASME J. Heat Transfer 113 (1991) 71–78.

Trainer, D.G., J. Kim, S.J. Kim, Heat transfer and flow characteristics of air-assisted impinging water jets, International Journal of Heat and Mass Transfer 64 (2013) 501513.

Usui, K., Sato, K., Vertically downward two-phase flow. (I). Void distribution and average void fraction, Journal of Nuclear Science and Technology, 26 (7) (1989) 670-680. doi:10.3327/jnst.26.670

Viskanta, R., Heat transfer to impinging isothermal gas and flame jets, Exp. Therm. Fluid Sci. 6 (1) (1993) 111-134.

Wang, E. N., L. Zhang, L. Jiang, J. M. Koo, K. E. Goodson, T. W. Kenny, J. G. Maveety, E. A. Sanchez, Micromachined Jet Arrays for Liquid Impingement Cooling of VLSI Chips, Solid-State Sensor, Actuator and Microsystems Workshop, Hilton Head Island, South Carolina, 2002 June 2-6.

Watson, E.J., The radial spread of a liquid over horizontal plane, J. Fluid Mech. 20 (1964) 481–500.

Webb, B.W., C. F. Ma, Single-phase liquid jet impingement heat transfer, Adv. Heat Transfer 26 (1995) 105-217.

Wilson, R., Too much ice can prevent the plane from doing important things like 'changing altitude or direction? and 'staying airborne? Retrieved from https://www.news.com.au/travel/travel-advice/flights/why-some-planes-need-to-be-deiced-before-flying/news-story/f29c5c0467a4ad888453d991578c9deb# (2018).

Yan, X., N. Saniei, Heat transfer from an oblique impinging air jet to a flat plate, Int. J. Heat and Fluid Flow 8 (6) (1997) 591-599.

Zhao, J., R.E. Khayat, Spread of a non-Newtonian liquid jet over a horizontal plate, J. Fluid Mech. 613 (2008) 411–443.

Zhao, Y., The cooling of a hot steel plate by an impinging water jet, PhD thesis, School of Mechanical, Materials and Mechatronics, University of Wollongong, (2005). http://ro.uow.edu.au/theses/450

Zuckerman, N., and N. Lior. "Jet Impingement Heat Transfer: Physics, Correlations, and Numerical Modeling." Advances in Heat Transfer (2006): 565-631.

Zumbrunnen, D.A., M. Balasubramanian, Convective heat transfer enhancement due to gas injection into an impinging liquid jet, ASME J. Heat Transfer 117 (1995) 1011-1017.